Geoscience Frontiers 12 (2021) 101178

HOSTED BY

Contents lists available at ScienceDirect

Geoscience Frontiers

journal homepage: www.elsevier.com/locate/gsf

Research Paper

Electrical properties of dry polycrystalline olivine mixed with various chromite contents: Implications for the high conductivity anomalies in subduction zones

Wenqing Sun [a], Jianjun Jiang [a], Lidong Dai [a,b,*], Haiying Hu [a,b], Mengqi Wang [a,c], Yuqing Qi [a,c], Heping Li [a]

[a] Key Laboratory of High-Temperature and High-Pressure Study of the Earth's Interior, Institute of Geochemistry, Chinese Academy of Sciences, Guiyang 550081, China
[b] Shandong Provincial Key Laboratory of Water and Soil Conservation and Environmental Protection, College of Resources and Environment, Linyi University, Linyi 276000, China
[c] University of Chinese Academy of Sciences, Beijing 100049, China

ARTICLE INFO

Article history:
Received 16 December 2020
Received in revised form 6 February 2021
Accepted 14 February 2021
Available online 27 February 2021

Handling Editor: K. Szilas

Keywords:
Electrical conductivity
Chromite
Olivine
High pressure
Conduction mechanism
High conductivity anomaly

ABSTRACT

Chromite, a crucial high-conductivity mineral phase of peridotite in ophiolite suites, has a significant effect on the electrical structure of subduction zones. The electrical conductivities of sintered polycrystalline olivine containing various volume percents of chromite (0, 4, 7, 10, 13, 16, 18, 21, 23, 100 vol.%) were measured using a complex impedance spectroscopic technique in the frequency range of 10^{-1}–10^{6} Hz under the conditions of 1.0–3.0 GPa and 873–1223 K. The relationship between the conductivities of the chromite-bearing olivine aggregates and temperatures conformed to the Arrhenius equation. The positive effect of pressure on the conductivities of the olivine–chromite systems was much weaker than that of temperature. The chromite content had an important effect on the conductivities of the olivine–chromite systems, and the bulk conductivities increased with increasing volume fraction of chromite to a certain extent. The inclusion of 16 vol.% chromites dramatically enhanced the bulk conductivity, implying that the percolation threshold of interconnectivity of chromite in the olivine–chromite systems is ~16 vol.%. The fitted activation enthalpies for pure polycrystalline olivine, polycrystalline olivine with isolated chromite, polycrystalline olivine with interconnected chromites, and pure polycrystalline chromite were 1.25, 0.78–0.87, 0.48–0.54, and 0.47 eV, respectively. Based on the chemical compositions and activation enthalpies, small polaron conduction was proposed to be the dominant conduction mechanism for polycrystalline olivine with various chromite contents. Furthermore, the conductivities of polycrystalline olivine with interconnected chromite ($10^{-1.5}$–$10^{0.5}$ S/m) provides a reasonable explanation for the high conductivity anomalies in subduction-related tectonic environments.

1. Introduction

According to the magnetotelluric (MT) data, high-electrical-conductivity layers are widely distributed in the Earth's subduction-related tectonic environments (Baba et al., 2006; Matsuno et al., 2010, 2020; Xiao et al., 2013; Xie et al., 2016; Li et al., 2020). Electrical conductivity is highly sensitive to material compositions and is thus considered to be a significant parameter to infer the origin of high conductivity anomalies in the Earth's interior (Dai and Karato, 2014a,b; Pommier et al., 2015; Hu et al., 2017; Shen et al., 2020). The conductivities of most dominant minerals and rocks in the deep Earth have been extensively investigated in previous studies (Wang et al., 2010; Manthilake et al., 2015, 2016; Dai et al., 2016, 2018, 2020; Sun et al., 2017; Hu et al., 2018; Dai and Karato, 2020). Comparing the laboratory results and MT data, the high conductivity anomalies in the subduction zones may be caused by various high-conductivity phases (e.g., saline fluids, high-conductivity minerals, or silicate or carbonate melts) (Bagdassarov et al., 2009; Wang et al., 2013a,b; Laumonier et al., 2015; Padilha et al., 2015; Guo and Keppler, 2019; Karato, 2019). Combined with the complicated geological environments in the Earth's interior, it is plausible that the high-conductivity layers in the various regions could be caused by different material compositions. However, the relationship between chromite, a crucial high-conductivity mineral phase, and the high conductivity anomalies in the subduction zones remains unclear.

Chromite is widely distributed within the outcrops of the mantle peridotites in ophiolites, and abundant chromic iron ores with high-grade chromite are widely distributed on a global scale (Page and Barnes, 2009; Torabi, 2009; Zhou et al., 2014; Arguin et al., 2016; Zhang et al., 2017; Rollinson et al., 2018; Uysal et al., 2018; Zhang et al., 2020).

* Corresponding author at: Key Laboratory of High-Temperature and High-Pressure Study of the Earth's Interior, Institute of Geochemistry, Chinese Academy of Sciences, Guiyang 550081, China; Shandong Provincial Key Laboratory of Water and Soil Conservation and Environmental Protection, College of Resources and Environment, Linyi University, Linyi 276000, China.
E-mail address: dailidong@vip.gyig.ac.cn (L. Dai).

https://doi.org/10.1016/j.gsf.2021.101178

There are three traditional viewpoints for the formation mechanisms of chromitites: interaction between mantle peridotite (especially harzburgite) and the melt in the upper mantle, partial melting of mantle peridotite and crystal fractionation, and mixing of Cr-enriched mafic magmas (Zhou et al., 1996; Arai and Miura, 2016). Podiform chromite deposits are defined as irregular, but fundamentally lenticular, chromite-rich bodies found within mantle peridotites of ophiolite complexes (Thayer, 1964; Dickey, 1975). Mantle sequences of many ophiolites contain podiform chromitites, which coexist with chromite ± olivine ± other silicate phases (Zhou et al., 2014). According to photographs of the natural chromitite specimens, the volume percents of chromite grains can exceed 50 vol.% (Zhou et al., 2014; Rollinson et al., 2018; Zhang et al., 2020). Olivine, the main co-existing mineral of chromite, is also the dominant mineral in the upper mantle, where the olivine volume fraction is ~60 vol.% (Ringwood, 1975, 1982; Lin et al., 2013). The electrical conductivities of single-crystal and polycrystalline olivine with various iron and water contents have been systematically investigated in previous studies (Dai et al., 2008; Dai and Karato, 2014a,b,c,d; Liu et al., 2017). The presence of hydrogen-related defects in olivine crystals was proposed as a possible origin of the high conductivity anomalies (Dai and Karato, 2014a). In addition, previous studies have evaluated the conductivities of olivine aggregates with high-conductivity phases (e.g., graphite, magnetite, iron sulfide) and revealed a significant effect of the high-conductivity phase on the conductivities (Wang et al., 2013a,b; Zhang and Pommier, 2017; Dai et al., 2019). However, the conductivities of olivine aggregates with chromites have not been reported. To determine the origins of the high conductivity anomalies in detail, it is necessary to investigate of the conductivities of olivine–chromite systems with various chromite contents at high temperatures and pressures.

In the present study, we measured the electrical conductivities of polycrystalline olivine with various chromite contents in situ under the conditions of 1.0–3.0 GPa and 873–1223 K. The effects of temperature, pressure and chromite content on the conductivities of the samples were systematically investigated. Based on the activation enthalpies, we also explored the conduction mechanisms for the samples in detail. Furthermore, the conductivities of polycrystalline olivine with interconnected chromite reasonably explained the high conductivity anomalies in the subduction zones.

2. Experimental procedures

2.1. Sample preparation

The chemical compositions of the fresh and origin-unknown olivine and chromite were determined using a field-emission electron probe microanalyzer (EPMA) at the State Key Laboratory of Ore Deposit Geochemistry, Chinese Academy of Science (CAS), Guiyang, China. The weight percents of the oxides for major elements in the olivine and chromite are shown in Table 1, and the ionic valences of chromium and iron elements are expressed as +3 and +2, respectively. The olivine and chromite grains were ultrasonically cleaned in a mixture of distilled water, acetone, and ethanol and then ground to a powder (<100 mesh) in an agate mortar after being dried in a furnace at 473 K for 4 h. The densities of the olivine and chromite were approximately 3.4 and 4.6 g/cm^3, respectively, and the olivine and chromite powder (weight percent of chromite: 5, 10, 15, 20, 25, 30, 35, and 40 wt.%) were weighted using a high-precision electronic scale. The olivine and chromite powder were homogeneously mixed, and the volume percent of chromite at normal temperatures and pressures was 4, 7, 10, 13, 16, 18, 21, and 23 vol.%, respectively. The pure olivine, pure chromite powder, and mixed powder were loaded into a copper capsule with a 0.025-mm-thick Ni-foil liner and then hot pressed for 6 h in a multi-anvil high-pressure apparatus at 2.0 GPa and 873 K. The hydrothermally annealed samples were cut and polished into cylinders of 6-mm diameter and height and then ultrasonically cleaned again using a mixture of deionized water, acetone, and ethanol. The samples were then baked at 373 K for 12 h to eliminate any absorbed water to avoid affecting the electrical conductivity measurements.

2.2. Impedance measurements

We performed the electrical conductivity measurements using the YJ-3000t multi-anvil apparatus and Solartron-1260 impedance/gain-phase analyzer at the Key Laboratory of High-Temperature and High-Pressure Study of the Earth's Interior, Institute of Geochemistry, CAS, Guiyang, China. Fig. 1 presents a schematic illustration of the cross section of the experimental assemblage for the electrical conductivity measurements at high temperatures and pressures. All the components of the sample assembly (pyrophyllite cubes, pyrophyllite plugs, ceramic tubes, MgO plugs, and Al_2O_3 and MgO sleeves) were baked at 1073 K in a muffle furnace for 8 h before the electrical conductivity measurements. In the sample assembly, a pyrophyllite cube (32.5 mm × 32.5 mm × 32.5 mm) and three-layer stainless-steel sheets (total thickness: 0.5 mm) were applied as the pressure medium and heater, respectively. Alumina and magnesia sleeves were placed between the sample and heater as insulators. To shield against external electromagnetism and spurious signal interference, a sheet of nickel foil (thickness: 0.025 mm) was placed between the alumina and magnesia sleeves. The sample was loaded into the magnesia tube, and then, two nickel disks (diameter: 6.0 mm and thickness: 0.5 mm) were placed on the top and bottom of the sample as electrodes. Before the electrical conductivity measurements, the sample assembly was heated in an oven at 323 K to avoid the effect of moisture.

The complex impedance spectra of the samples (frequency range: 10^{-1}–10^6 Hz and applied voltage: 1 V) were collected under conditions of 1.0–3.0 GPa and 873–1223 K. In the experiments, the pressure was slowly raised to a designated pressure at a speed of 1.0 GPa/h, and then, the temperature was increased to 873 K at a rate of 50 K/min. When the desired temperatures and pressures remained stable, the complex spectra were measured. Then, the temperature was increased to another desired value at an interval of 50 K, and the complex spectra were collected again. To obtain reproducible data, the electrical conductivities of the samples were measured in multiple heating/cooling cycles under the experimental conditions. The experimental temperatures were monitored with a K-type thermocouple (NiCr/NiSi). The errors of temperature and pressure were ±5 K and ±0.1 GPa, respectively.

The internal composition and structure of the recovered samples with chromite contents of 4, 7, 10, 13, 16, 18, 21, and 23 vol.% are shown in Fig. 2 (these measurements were conducted using a scanning electron microscope at the Center for Lunar and Planetary Sciences, Institute of Geochemistry, CAS, Guiyang, China). The olivine and chromite grains were homogeneously distributed in the samples. The shapes of the olivine and chromite were irregular, and the grain sizes of olivine

Table 1
The contents of main elements in the initial samples of olivine and chromite revealing by the weight percents (wt.%) of the corresponding oxides, where all iron ions were assumed to be ferrous ions.

Sample	FeO	MnO	NiO	Cr_2O_3	Al_2O_3	TiO_2	Na_2O	SiO_2	MgO	K_2O	CaO	As_2O_5	V_2O_3	Total
Olivine	9.158	0.117	0.376	0.003	0.000	0.000	0.003	45.439	44.351	0.001	0.036	0.000	0.000	99.484
Chromite	25.515	0.280	0.087	47.246	14.908	0.577	0.000	0.000	10.349	0.000	0.000	0.088	0.370	99.420

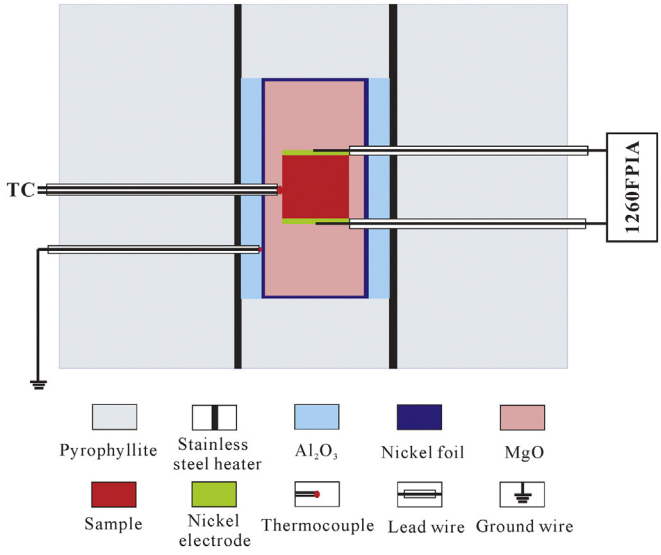

Fig. 1. Schematic illustration of cross-section of sample assembly for high-*P*/*T* electrical conductivity measurements.

and chromite in a recovered sample varied (long axis: less than 150 μm). However, the ranges of grain size in various samples were very close. Thus, the possible differences in the electrical conductivities of the various olivine–chromite systems cannot be caused by the grain size. To determine the water contents of the olivines before and after the electrical conductivity measurements, we applied Fourier-transform infrared (FTIR) spectroscopy (Vertex-70V and Hyperion-1000 infrared microscope at the Key Laboratory of High-temperature and High-pressure Study of the Earth's Interior, Institute of Geochemistry, Chinese Academy of Sciences, China). The samples with less than 200-μm thickness were placed on a CaF_2 window, and the absorbances of the mid-IR lights were detected by a mercury-cadmium-telluride detector (aperture size: 100 μm × 100 μm). For the original and recovered samples, at least 5 infrared spectra from different positions for each sample were collected using unpolarized radiation. The absorbance in the wavenumber range of 3000–4000 cm^{-1} with 512 scans was obtained, and the infrared spectra after simple base and smooth treatments are shown in Fig. 3. No obvious absorption peak appeared in the infrared spectra of the original and recovered olivine samples, implying that the olivine before and after the electrical conductivity measurements was almost dry.

3. Results

The impedance spectra of the pure polycrystalline olivine and olivine–chromite system with 18 vol.% chromites consisted of an approximate semicircle in the higher-frequency region of 10^3–10^6 Hz and an additional tail in the lower-frequency region of 10^{-1}–10^3 Hz (Fig. 4). The shapes of the impedance spectra for the other olivine–chromite systems with various chromite contents were similar to those in Fig. 4b. According to the theory of complex impedance spectra and previous relevant studies, the ideal semicircle in the high-frequency region is related to the conduction process for the samples, and the additional tail is related to the diffusion processes of inductive reactance at the sample–electrode interface (Roberts and Tyburczy, 1991; ten Grotenhuis et al., 2004; Wang et al., 2013a,b; Pommier et al., 2018). Therefore, the bulk resistance of our samples was obtained by fitting the ideal semicircle in the high-frequency region. A parallel connection of R_S-CPE_S (R_S and CPE_S represent the resistance and constant-phase element of the sample, respectively) was applied as the equivalent circuit, and the fitting errors of the electrical resistance were less than 10%. For the measuring method using two electrodes consisting of parallel plates, the electrical conductivities of the samples were calculated using the following formula:

$$\sigma = G/R_S \quad (1)$$

where G is the sample geometric constant calculated based on L/S (L is the height of the sample (m) and S is the cross-sectional area of the electrodes (m^2)), R_s is the fitting resistance (Ω), and σ is the electrical conductivity of the sample (S/m).

To obtain reproducible data, the conductivities of the samples were measured in multiple sequential heating and cooling cycles at certain pressures. As shown in Fig. 5, after the first heating process, the conductivities of the sample in different heating/cooling cycles were close to each other. This result indicated that the polycrystalline samples remained in a steady state after the first heating cycle. We used reproducible data to investigate the electrical properties of dry olivine aggregates with various chromite contents. The logarithmic electrical conductivities of the dry polycrystalline olivine with certain chromite contents were plotted against the reciprocal temperatures under the conditions of 1.0–3.0 GPa and 873–1223 K. The electrical conductivities of polycrystalline olivine mixed with 16 vol.% chromite slightly increased with increasing pressure (Fig. 6). In addition, the conductivities of the olivine aggregates with 4 vol.% chromite was much higher than those of the pure polycrystalline olivine, and the chromite slightly enhanced the conductivities of the olivine–chromite systems when the volume fraction of chromite was 4–10 vol.%. The electrical conductivities of the olivine–chromite system with 13 vol.% chromite were moderately higher than those of the sample with 10 vol.% chromite. There was an inflection point in the variation trend for the sample conductivities when the chromite content reached 16 vol.%. The conductivities of the samples then moderately increased with increasing chromite content (16–23 vol.%) (Figs. 7 and 8). For the polycrystalline olivine–chromite system with 16 vol.% chromite, the chromite was finely interconnected based on the change trend of the electrical conductivity (Fig. 8). Interconnected chromite can dramatically enhance the conductivities of olivine aggregates. At a certain pressure, the relationship between the electrical conductivities of all the samples and temperatures were fitted to the Arrhenius formula:

$$\sigma = \sigma_0 \exp(-\Delta H/kT) \quad (2)$$

where σ_0 is the pre-exponential factor (K·S/m), k is the Boltzmann constant (eV/K), T is the absolute temperature (K), and ΔH is the activation enthalpy (eV). All the fitting parameters for the electrical conductivities of the olivine aggregates with various chromite contents are listed in Table 2. The activation enthalpy for pure polycrystalline olivine was determined to be 1.25 eV, and that for polycrystalline olivine mixed with isolated and interconnected chromite was 0.78–0.87 eV and 0.48–0.54 eV, respectively. For pure polycrystalline chromite, the activation enthalpy was 0.47 eV under the conditions of 2.0 GPa and 873–1223 K. Furthermore, the logarithmic pre-exponential factors for all the samples were positive.

4. Discussion

4.1. Comparison with previous studies

The electrical conductivities of polycrystalline olivine containing 16 vol.% chromites in the first heating cycle were lower than those in the first cooling cycle and second heating/cooling cycle (Fig. 5). This result indicates that the polycrystalline olivines with a certain chromite content were unstable in the first heating cycle. During the first heating cycle, the chemical compositions of olivine and chromite might be slightly changed, and microcracks gradually tend closed. The electrical conductivities of the polycrystalline olivine with a certain chromite content showed good repeatability after the first heating cycle, indicating

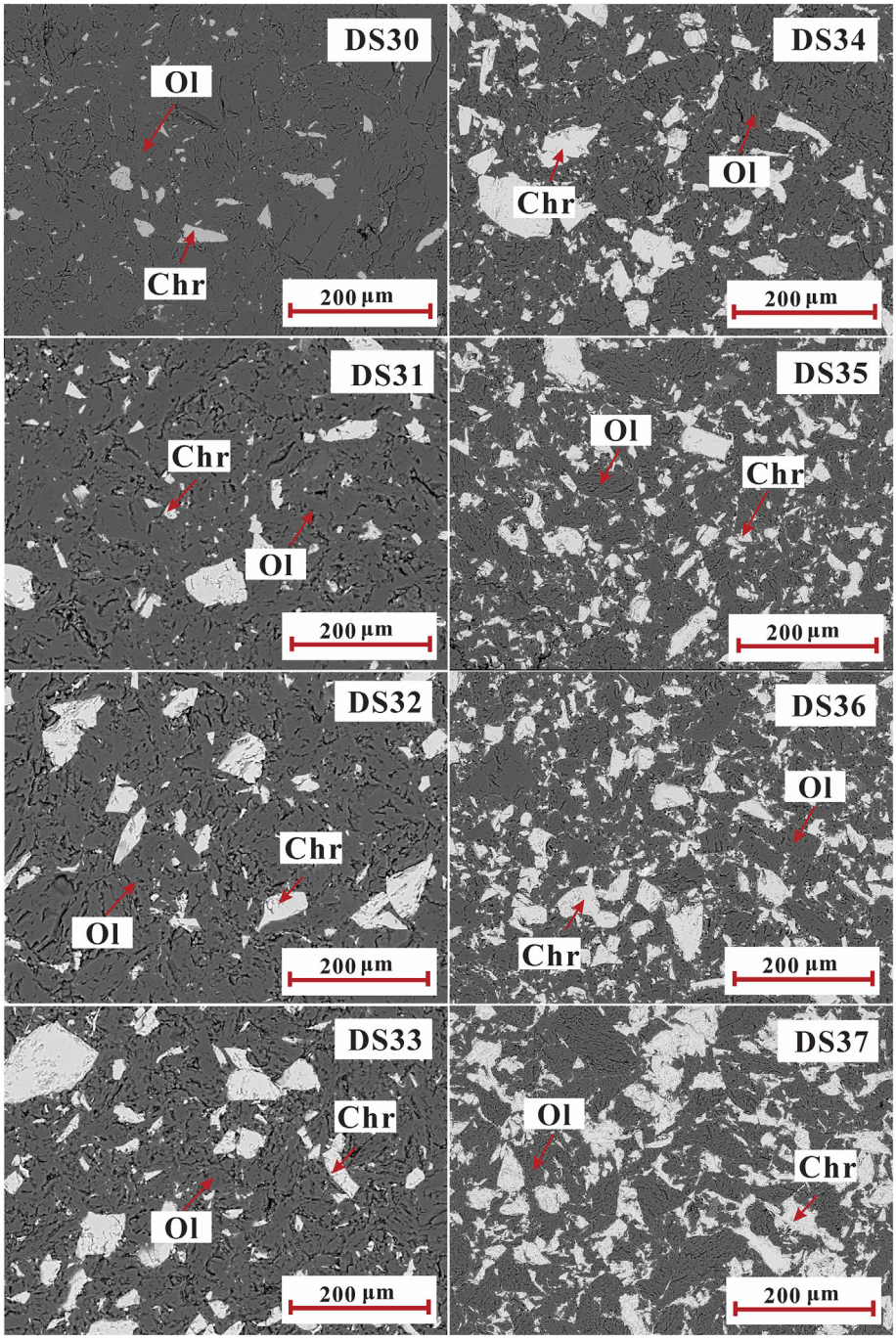

Fig. 2. Back-scattered electron images of recovered samples of polycrystalline olivine–chromite systems containing various volume percents of chromite. The chromite contents for the DS30, DS31, DS32, DS33, DS34, DS35, DS36, and DS37 run were 4, 7, 10, 13, 16, 18, 21, and 23 vol.%, respectively.

that the samples remained stable. Previous studies have shown that the electrical conductivities of silicate minerals and rocks are unstable in the previous heating/cooling cycles and gradually remain stable in the subsequent heating/cooling cycles (Wang et al., 2010; Hu et al., 2015; Dai et al., 2018, 2019). These phenomena imply that the interior of most minerals and rocks undergo little change even if there is no phase transition at high temperatures and pressures. During this process, the grain size, element distribution, and porosity will change to some extent and gradually reach steady state.

Under the conditions of 2.0 GPa and 873–1223 K, the electrical conductivities of the pure polycrystalline olivine and polycrystalline olivines with isolated chromite were approximately 10^{-5}–10^{-3} and 10^{-4}–$10^{-2.5}$ S/m, respectively; the conductivities of the polycrystalline olivine with interconnected chromite and pure polycrystalline chromite were $10^{-1.5}$–$10^{0.5}$ and 10^{1}–$10^{1.5}$ S/m, respectively (Fig. 7). Based on the conductivities of the pure olivine and chromite aggregates and the volume fraction of olivine and chromite grains in the olivine–chromite systems, we applied the computational formulas of the Hashin–Shtrikman models to calculate the upper and lower bounds (HS^{+} and HS^{-}) of the electrical conductivities for the olivine–chromite systems (Hashin and Shtrikman, 1962) (Table 3). As shown in Fig. 7 and Table 3, the experimental results of the conductivities of the olivine–chromite systems were much higher than the lower bounds and much lower than the upper bounds from the Hashin–Shtrikman models.

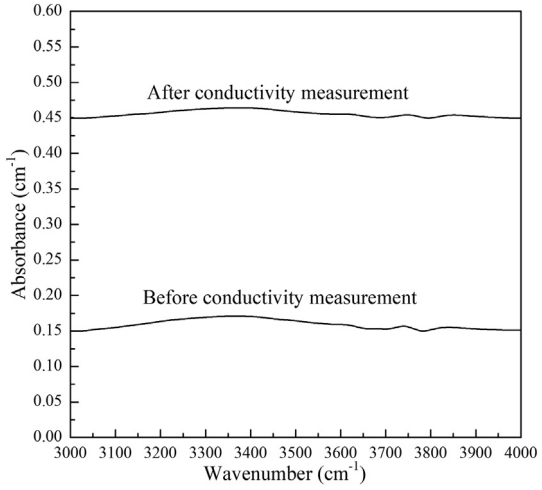

Fig. 3. Fourier-transform infrared (FTIR) spectra of olivines before and after electrical conductivity measurements in the wavenumber range of 3000–4000 cm^{-1}.

This discrepancy might be caused by the differences in the particle shape, grain size, and mineral distribution of the samples in this study and in the HS models. The HS models can be used to constrain the upper and lower bounds for the conductivities of the samples but cannot be used to calculate accurate conductivities of the olivine–chromite system. Thus, we applied our experimental data to investigate the effect of temperature, pressure, and chromite content on the conductivities of the olivine–chromite system. As shown in Fig. 8, the conductivities of the olivine–chromite system slightly increased with increasing chromite content from 4 vol.% to 10 vol.%; the conductivities of the system containing 13 vol.% chromites were moderately higher than those of the system containing 10 vol.% chromites but much lower than those of the system containing 16 vol.% chromites. According to previous studies, for polycrystalline minerals mixed with a high-conductivity phase, the isolated high-conductivity phase slightly enhanced the electrical conductivities; however, the conductivities were dramatically increased when the high-conductivity phase reached a state of interconnection (Dai et al., 2019). The inflection point of the relationship between the sample conductivities and contents of the high-

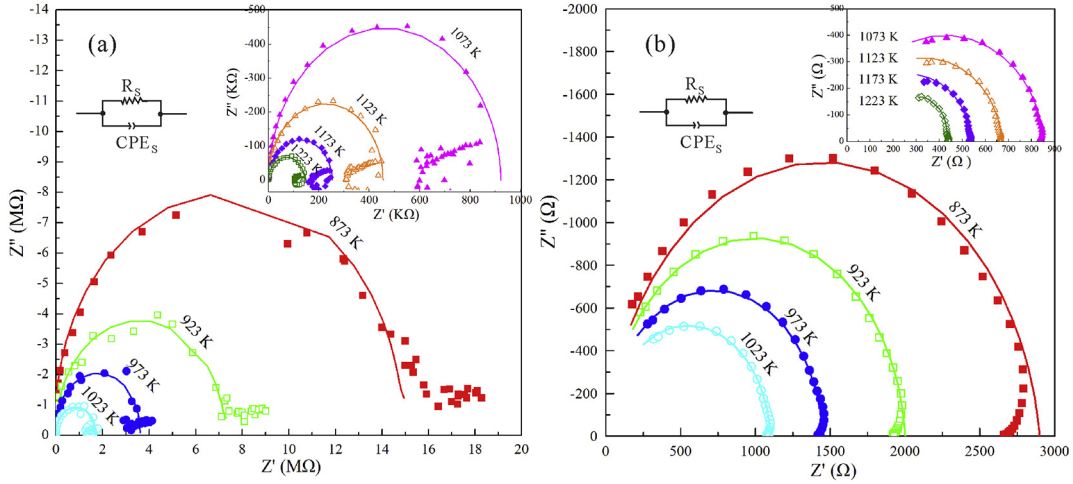

Fig. 4. Representative complex impedance spectra for (a) pure polycrystalline olivine and (b) olivine–chromite system containing 18 vol.% chromite under the conditions of 2.0 GPa and 873–1223 K.

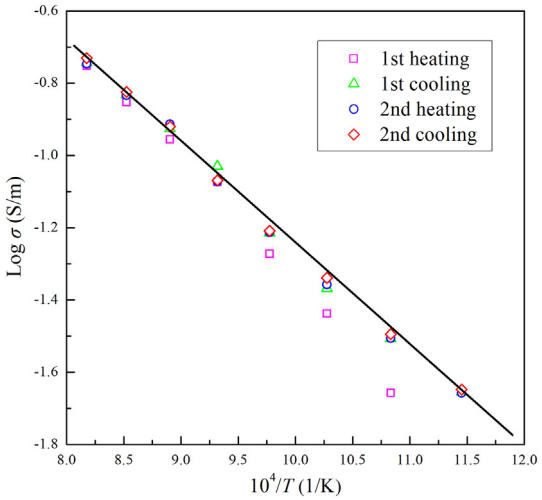

Fig. 5. Logarithmic electrical conductivity versus reciprocal temperature for olivine–chromite system containing 16 vol.% chromite during two heating/cooling cycles under the conditions of 2.0 GPa and 873–1223 K.

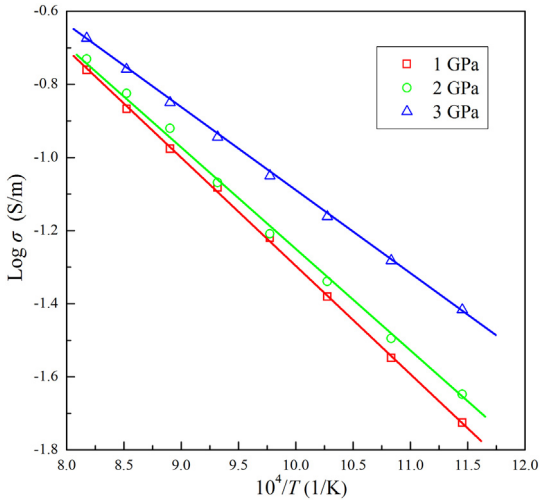

Fig. 6. Linear relationship between logarithmic electrical conductivity and reciprocal temperature for olivine–chromite system containing 16 vol.% chromites under the conditions of 1.0–3.0 GPa and 873–1223 K.

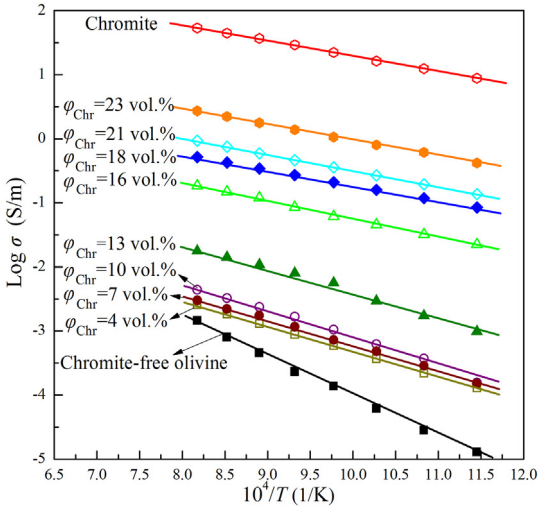

Fig. 7. Logarithm of electrical conductivity versus reciprocal temperature for olivine aggregates containing various chromite contents at 2.0 GPa and 873–1223 K.

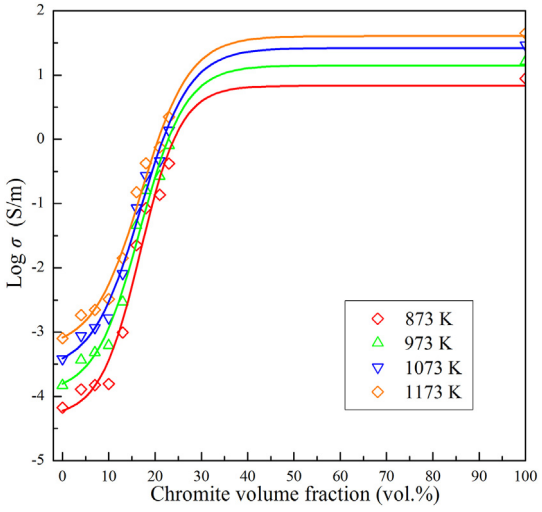

Fig. 8. Relationship between electrical conductivity and chromite volume fraction for the olivine–chromite systems at 2.0 GPa and 873–1173 K. The relation curves were fitted with the Boltzmann function in the OriginPro 8 software.

Table 2
Fitted parameters of the Arrhenius relation for the electrical conductivity of the olivine samples with various chromite contents.

Run No.	φ_{Ilm} (vol.%)	P (GPa)	T (K)	Logσ_0 (S/m)	ΔH (eV)	R^2
DS29	0	2.0	873–1223	2.23 ± 0.10	1.25 ± 0.02	99.81
DS30	4	2.0	873–1223	0.62 ± 0.03	0.78 ± 0.01	99.94
DS31	7	2.0	873–1223	0.93 ± 0.08	0.83 ± 0.01	99.69
DS32	10	2.0	873–1223	1.27 ± 0.08	0.87 ± 0.02	99.67
DS33	13	2.0	873–1223	1.54 ± 0.10	0.79 ± 0.01	99.41
DS34	16	2.0	873–1223	1.48 ± 0.04	0.54 ± 0.01	99.74
DS35	18	2.0	873–1223	1.68 ± 0.01	0.48 ± 0.01	99.98
DS36	21	2.0	873–1223	2.02 ± 0.02	0.50 ± 0.01	99.94
DS37	23	2.0	873–1223	2.52 ± 0.03	0.51 ± 0.01	99.89
DS38	100	2.0	873–1223	3.65 ± 0.04	0.47 ± 0.01	99.78

conductivity phase was considered to be the approximate percolation threshold (Dai et al., 2019). Thus, we proposed that the percolation threshold of the chromite in the olivine–chromite systems was ~16 vol.%. The conductivities of polycrystalline olivine with isolated chromite were moderately higher than those of the pure olivine aggregates, and the interconnected chromites significantly affected the conductivities of the olivine–chromite systems. In addition, the electrical conductivities of the polycrystalline olivine containing various chromite contents moderately increased with increasing temperatures and slightly changed with rising pressures. These phenomena are similar to those observed for most silicate minerals and rocks at high temperatures and pressures (Xu et al., 2000; Wang et al., 2010; Hu et al., 2014; Hui et al., 2015; Dai et al., 2016, 2018; Manthilake et al., 2016). The effect of pressure on the conductivities of the pure polycrystalline olivine was negative (Dai et al., 2010); however, the conductivities of the olivine–chromite systems in this study and the olivine–magnetite systems of Dai et al. (2019) increased with increasing pressure. Thus, the pressure effect for the conductivities of pure polycrystalline olivine was opposite to that of olivine aggregates containing some high-conductivity mineral phases. According to previous studies, the content of important high-conductivity phases (e.g., graphite, FeS, and magnetite) significantly affects the conductivities of mantle peridotite (Wang et al., 2013a,b; Zhang and Pommier, 2017; Dai et al., 2019). As shown in Fig. 9, the electrical conductivities of the pure polycrystalline olivine in this study were slightly higher than those of the olivine aggregates of Dai et al. (2019) but moderately lower than those of Zhang and Pommier (2017). The olivine samples of this study and those of Dai et al. (2019) and Zhang and Pommier (2017) were anhydrous; thus, the electrical conductivity differences might be caused by the various iron contents, as the iron content was shown to have a significant effect on the electrical conductivities of dry olivine (Dai and Karato, 2014b). For the olivine aggregates with graphite, the conductivities were markedly enhanced when the concentration of graphite exceeded the percolation threshold of ~4 vol.% (Wang et al., 2013a,b). The percolation threshold for graphite (~4 vol.%) was much lower than that for chromite (~16 vol.%). The electrical conductivities of the olivine–4 vol.% graphite system were approximately 0.5–1 orders of magnitude lower than those of the olivine–16 vol.% chromite system. The conductivities of the olivine–16 vol.% chromite system were close to those of the olivine–12 vol.% FeS system but slightly lower than those of the olivine–3 vol.% magnetite system. Furthermore, the conductivities of the olivine–7 vol.% graphite system were ~2.5–3 orders of magnitude higher than those of the olivine–3 vol.% magnetite system. It was proposed that the different effect degrees of various high-conductivity mineral phases on the bulk conductivities were due to the various conductivities and interconnectivity of the impurity phases.

4.2. Conduction mechanism

For olivine aggregates with various chromite contents, the logarithmic electrical conductivities and reciprocal temperatures conformed to linear relationships under the experimental conditions of 1.0–3.0 GPa and 873–1223 K. This finding indicated that the conduction process of the samples was under the control of one dominant conduction mechanism. Small polarons, protons, and ions are proposed to be the significant charge carriers for silicate minerals and rocks (Wang et al., 2010; Manthilake et al., 2016; Hu et al., 2018). The material compositions were important factors determining the conduction mechanism of the samples. As shown in Table 1, the calcium and alkaline ions in the pure and fresh olivine and chromite crystals can be ignored because of their very minor content. Thus, impurity ionic conduction cannot be the conduction mechanism for the pure olivine aggregates and polycrystalline olivine containing various chromite contents. Dai and Karato (2014b) investigated the electrical conductivities of hydrous olivine aggregates, and the activation enthalpies for proton-related impurity ion conduction were 0.8–0.88 eV, which were much lower than the activation enthalpy for olivine aggregates (1.25 eV) in this study. In addition, there was almost no hydrogen in the olivine aggregates according to the FT-IR spectra. It was thus implied that proton conduction could not be the conduction mechanism for the samples. The activation

Table 3
The calculated logarithmic conductivities (Logσ, unit: S/m) of the olivine–chromite systems under the conditions of 2.0 GPa and 873–1223 K using the Hashin-Shtrikman upper (HS^+)- and lower (HS^-)-bound models. Ol and Chr are abbreviations of olivine and chromite, respectively.

T (K)	Ol	Chr	HS^+						HS^-			
			Chr- 7 (vol.%)	10	13	16	23	7	10	13	16	23
873	−4.89	0.95	−0.37	−0.21	−0.09	0.00	0.17	−4.80	−4.77	−4.73	−4.70	−4.61
923	−4.55	1.10	−0.22	−0.06	0.08	0.15	0.32	−4.46	−4.43	−4.39	−4.35	−4.27
973	−4.21	1.21	−0.11	0.05	0.17	0.26	0.43	−4.12	−4.09	−4.05	−4.01	−3.93
1023	−3.86	1.35	0.03	0.19	0.31	0.40	0.57	−3.77	−3.74	−3.70	−3.66	−3.58
1073	−3.63	1.47	0.15	0.31	0.43	0.52	0.69	−3.54	−3.51	−3.47	−3.43	−3.35
1123	−3.34	1.57	0.25	0.41	0.53	0.62	0.79	−3.25	−3.22	−3.18	−3.14	−3.06
1173	−3.10	1.65	0.33	0.49	0.61	0.70	0.87	−3.01	−2.98	−2.94	−2.90	−2.82
1223	−2.83	1.73	0.41	0.57	0.69	0.78	0.95	−2.74	−2.71	−2.67	−2.63	−2.55

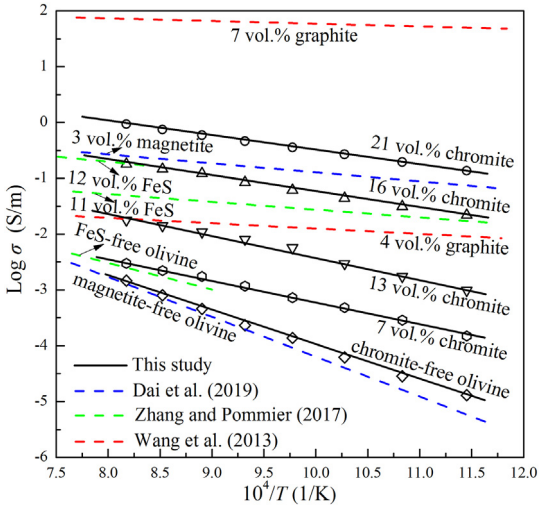

Fig. 9. Comparisons of the electrical conductivities of the olivine–chromite systems measured at 2.0 GPa in this study with the data measured for olivine–graphite systems, olivine–FeS systems, and olivine–magnetite systems in previous studies. The dashed red lines represent the conductivities of olivine aggregates containing 4 vol.% and 7 vol.% graphite at 4.0 GPa (Wang et al., 2013a,b), the dashed green lines represent the conductivities of FeS-free olivine aggregates and olivine–FeS systems containing 11 vol.% and 12 vol.% FeS at 4.7–6.1 GPa (Zhang and Pommier, 2017), and the dashed blue lines represent the conductivities of magnetite-free olivine aggregates and olivine–magnetite system containing 3 vol.% magnetite at 2.0 GPa (Dai et al., 2019).

enthalpy for the dry polycrystalline olivine (1.25 eV) in this study was close to that of the dry olivine aggregates with small polaron conduction mechanism (1.21–1.48 eV) (Dai and Karato, 2014b). Therefore, we proposed that small polaron conduction was the main conduction mechanism for the pure polycrystalline olivine. For polycrystalline olivine with isolated chromite, the electrical conductivity was dominated by the olivine, and thus, the main conduction mechanism was small polaron conduction. Chromite dominated the conductivities of the olivine–chromite systems when the chromite grains remained interconnected. Iron and chromium ions, as variable valence elements, occupied the lattice positions of chromite $(Fe,Mg)Cr_2O_4$, and the valence states of Fe^{2+} and Cr^{3+} could be changed to 3+ and 2+, respectively. This indicated that electrons in the conduction band of Fe^{2+} migrated to the electron vacancies of Cr^{3+} at a certain excitation voltage (Fig. 10). Thus, small polaron conduction was proposed to be the conduction mechanism for the chromites. In addition, a small polaron as a charge carrier may possibly migrate through the olivine and chromite grain boundary (Fig. 10). The mechanism for small polaron conduction (Schock et al., 1989; Hirsch et al., 1993; Dai et al., 2016) was revealed to be the following:

$$Fe^{\times}_{Mg} + h^{\bullet} \rightleftharpoons Fe^{\bullet}_{Mg} \quad (3)$$

where $Fe^{\times}_{Mg}$ and $Fe^{\bullet}_{Mg}$ represent the ferrous and ferric ions occupying the lattice site in olivine, respectively, and $h^{\bullet}$ is the electron hole in the outmost electronic shell for iron ions. The electrical conductivity of minerals and rocks can be described by the Nernst–Einstein equation (Xu and McCammon, 2002; Karato, 2013):

$$\sigma = \sum_j n_j q_j \mu_j \quad (4)$$

where σ is the electrical conductivity of the sample, n_j is the concentration of j-type charge carriers, q_j is the effective charge, and μ_j is the

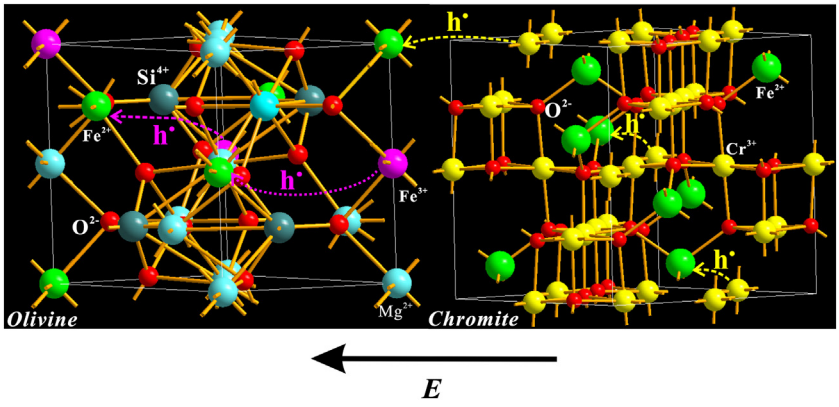

Fig. 10. Schematic diagrams of the conduction mechanism for small polarons in the olivine–chromite systems. The colored balls represent ions occupying the lattice positions of the olivine and chromite crystals, and the balls of the same color indicate one type of ion. The names of the ions are shown next to the balls. It is noted that Mg^{2+} in the chromite crystal can occupy the position of Fe^{2+}; however, Mg^{2+} does not participate in the conduction process. *E* represents the electrical field along the direction indicated by the arrow, and $h^{\bullet}$ is a hole transported from Fe^{3+} and Cr^{3+} to Fe^{2+} in the olivine and chromite crystals.

charge mobility. Because of the short bond length and high concentration of Fe^{2+} and Cr^{3+}, the concentration of small polarons in the chromite was much higher than that in the olivine, and the activation enthalpy for chromite aggregates (0.47 eV) was much lower than that for olivine aggregates (1.25 eV) at high temperatures and pressures. Furthermore, the main ions exchanged between olivine and chromite might be Fe^{2+}, Mg^{2+}, Cr^{3+}, and Mn^{2+}, which will not affect the species of the charge carriers (small polaron) in the olivine–chromite systems. The molar concentrations of the charge carriers in the olivine and chromite might be slightly changed.

5. Geophysical implication

Chromite is a significant metallic mineral in the peridotites of the depleted oceanic or subcontinental lithosphere (Yamamoto et al., 2009; Arai, 2010, 2013; Griffin et al., 2016). Ultrahigh-pressure (UHP) mineral inclusions (e.g., coesite, diamond) have been found in the chromitites ("UHP chromitites"), implying a much deeper origin for both chromitites and their host rocks (Yang et al., 2007). The low-pressure (upper mantle) igneous chromitites can be conveyed through mantle convection or subduction down to the mantle transition zone to form ultrahigh-pressure chromitites. The "subduction-recycling" model has been constructed to interpret the formation process of "UHP chromitites": A segment of the lithospheric mantle with low-pressure chromitites was subducted into the deep mantle and stagnated around the Transition Zone, where the diopside-associated chromite transformed into the CF-structured phase, with a strongly deformed and lineated microstructure (Arai, 2010, 2013; Satsukawa et al., 2015; Griffin et al., 2016). After a long residence (≥150 Ma), the depleted harzburgite was heated to the ambient mantle *T* and became more buoyant than the surrounding mantle and was then recycled back to shallow depth due to the effects of slab rollback and mantle convection (McGowan et al., 2015; Griffin et al., 2016). During the uplift process, the CF-structured phase transformed back into chromite at depths of approximately 400 km (Satsukawa et al., 2015), and the recycled mantle rocks with UHP chromites appeared in the harzburgite diapir (Griffin et al., 2016). Some of these UHP chromites reappeared in the shallower mantle and can coexist with newly formed low-pressure igneous chromitites. Based on the geological environments, the chromitites can be divided into Arc-type and mid-ocean ridge-type chromitites, and chromitites may be common beneath the ocean floor. High-temperature hydrothermal fluids can dissolve and precipitate chromite, and hydrothermal chromitites (chromitites precipitated from aqueous fluids) are possibly formed within the mantle where the circulation of hydrous fluid is available, e.g., at the mantle wedge (Arai and Miura, 2016). Furthermore, chromite deposits are widely distributed in the ophiolites of many subduction zones, e.g., Luobusha (SE Tibet), Thetford (E Canada), Guleman (SE Turkey), Othris (W Greece), and Oman (Page and Barnes, 2009; Zhang et al., 2016, 2017; Kapsiotis et al., 2018; Rollinson et al., 2018; Uysal et al., 2018; Zhang et al., 2020). The chromite content in the mantle-derived peridotite of the ophiolite suite is very large in some local regions (Zhou et al., 1996; Satsukawa et al., 2015; Rollinson et al., 2018). The high chromite content in the peridotite of ophiolite implies that abundant chromite might still be distributed in the deep Earth. Zhou et al. (2014) investigated the possible formation mechanism of the chromite deposit in the subduction zones (Fig. 11). Upward-migrating magmas reacted with the subducted materials in the slab window; the magmas become more silicious, more hydrous, and more oxidized, and thus, the crystallization of chromite was rapidly triggered (Matveev and Ballhaus, 2002). The newly formed chromite crystals in the hydrous magmas were entrained in rising melts, which would pass through suprasubduction zone (SSZ) mantle wedges (Zhou et al., 2014). The fine chromite grains can coalesce in the upward-migrating magmas (Matveev and Ballhaus, 2002) and be deposited as massive, nodular, and disseminated chromitites (Zhou et al., 2014). The chromite aggregates (chromitite) were widely distributed in the dunite according to field geological investigations (Zhou et al., 1996; Kim et al., 2020). It was indicated that olivine–chromite systems can represent the peridotite with abundant chromites in the subduction zones. The chromitites

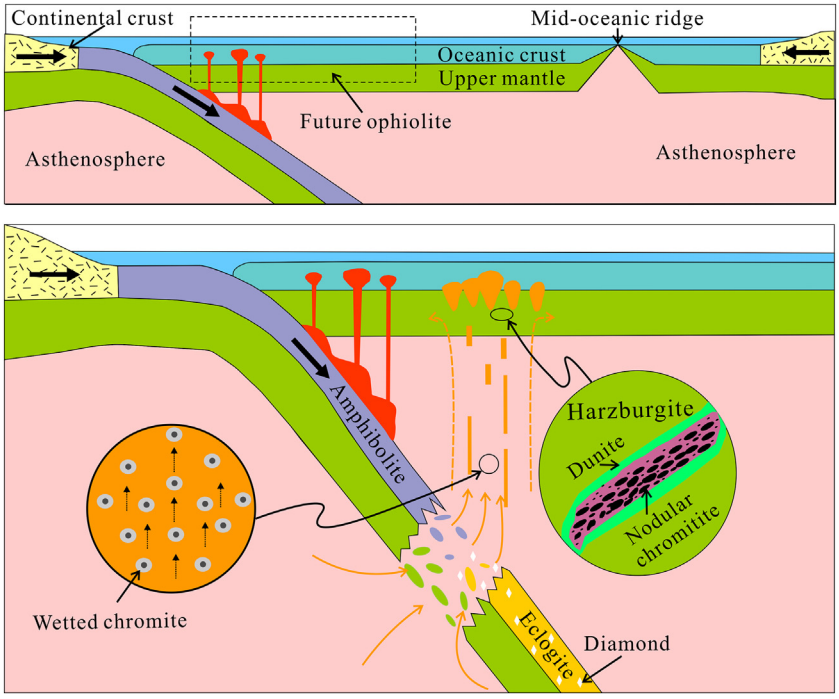

Fig. 11. A possible model for the formation of podiform chromitites from Zhou et al. (2014). Cr-rich upward-migrating magmas assimilated the slab window, and then wetted chromites with fine grains were formed due to the change of the chemical compositions and temperatures for the magmas. The wetted chromites coalesced in the upward-migrating magmas, forming podiform chromitites, which were distributed into the lithosphere above the subduction slabs.

might be formed by the differentiation of Cr-rich magma (Liu and O'Neill, 2004; Arai and Miura, 2016; Zhang et al., 2020), and the positions of chromite-rich peridotites possibly migrated as a result of the late tectonic movements. Thus, it was difficult to determine the concrete positions of chromite-rich peridotites in subduction zones based on the presumed geological environments. We have demonstrated that the presence of interconnected chromites significantly enhanced the conductivities of the dunite, and thus, the interconnected chromites might be closely related to the high conductivity anomalies in the subduction zones.

Magnetotelluric detection technology has been widely applied as a remote sensing method to determine the electrical structure in the Earth's crust and upper mantle. High conductivity anomalies beneath southern Tibet, Grenville province, Cascadia, and the Cocos plate have been observed based on the magnetotelluric data (Naif et al., 2013; Evans et al., 2014; Adetunji et al., 2015; Wang et al., 2017). Although the presence of silicate melts, carbonated melts, and aqueous fluids can be used to interpret the origin of high-conductivity layers (Wei et al., 2001; Gaillard et al., 2008; Laumonier et al., 2015, 2017; Hu et al., 2017; Sun et al., 2020), a significant influencing factor on the high conductivity anomalies, the chromite content, has not been reported in previous studies. To investigate the relationship between the high-conductivity layers and the presence of chromite, we compared the electrical conductivities of polycrystalline olivine–chromite systems and high-conductivity layers in representative geological environments. According to the thermal models in southern Tibet, Grenville province, Cascadia, and the Cocos plate (Mareschal et al., 1998; Currie et al., 2002, 2004; Wang et al., 2013a,b), the electrical conductivity–temperature data of polycrystalline olivine containing 16 and 23 vol.% chromites were converted into relevant electrical conductivity profiles (Fig. 12). With increasing depth, the electrical conductivities of polycrystalline olivine containing 23 vol.% chromites became higher than those of polycrystalline olivine containing 16 vol.% chromites. At the same depth, large differences in the electrical conductivities of polycrystalline olivine with interconnected chromites in different geological environments existed because of the various thermal structures (Fig. 12). Furthermore, the electrical conductivity–depth profiles of southern Tibet, Grenville province, Cascadia, and the Cocos plate were constructed using the corresponding magnetotelluric data (Naif et al., 2013; Evans et al., 2014; Adetunji et al., 2015; Wang et al., 2017). The electrical conductivities and depth ranges of the high-conductivity layers in the four regions were different because of the special geological evolutions. As shown in Fig. 12, the electrical conductivities of polycrystalline olivine containing 16 vol.% chromites were close to those of the largest conductivities of the high-conductivity layers in the Cocos plate. It was implied that the high conductivity anomalies in the Cocos plate could be caused by the mantle peridotite containing ≤16 vol.% chromites. The largest conductivity in the high-conductivity layers in Cascadia was close to the conductivity of polycrystalline olivine containing 23 vol.% chromites. Thus, the high conductivity anomalies in Cascadia might be caused by the presence of ≤23 vol.% chromites. For the high-conductivity layers in the Grenville province, the largest conductivity was close to those of polycrystalline olivine containing 23 vol.% chromites but much higher than those of the polycrystalline olivine containing 16 vol.% chromites. Thus, the high conductivity anomalies may be related to be the mantle peridotite containing ~23 vol.% chromites. The largest conductivity of the high-conductivity layer in southern Tibet was moderately higher than those of polycrystalline olivine containing 23 vol.% chromites. Therefore, the high conductivity anomalies in southern Tibet cannot be caused by the presence of interconnected chromites with a volume fraction of less than 23 vol.%. According to previous studies, the high conductivity anomalies in southern Tibet can be caused by the silicate melts and saline fluids (Guo et al., 2018; Sun et al., 2020). The origin of the high conductivities in the subduction zones has always been considered to be caused by a single high-conductivity phase (e.g., saline fluids, melts, or a high-conductivity mineral phase) (Wang et al., 2013a,b; Laumonier et al., 2015; Guo et al., 2018). However, chromite, silicate melts, and aqueous fluids might coexist in the host rocks (e.g., dunite and harzburgite) of the subduction zones and upper mantle (Matveev and Ballhaus, 2002; Zhou et al., 2014). Therefore, the origin of a high-conductivity layer might not be the presence of a single high-conductivity phase, and the dominant high-conductivity phases in various regions might differ. Interconnected chromites were proposed to be the possible material compositions of the high-conductivity layers in certain regions with abundant chromites of the subduction zones and upper mantle. In addition, the electrical anisotropy of the high-conductivity layers in the upper mantle is a significant geological phenomenon (Matsuno et al., 2010; Naif et al., 2013; Adetunji et al., 2015; Pommier et al., 2015). Two electrical layered models were applied to interpret the electrical anisotropy in the high-conductivity layers of the upper mantle (Pommier et al., 2015). However, no practical geological samples have confirmed that the layered melt with anisotropic connectivity rate was distributed in the mantle peridotite. The presence of podiform (or nodular) chromitites with oriented arrangement in the mantle peridotite might be a new crucial influencing factor on the electrical anisotropy in the upper mantle (Fig. 11). The conductivities of peridotite with podiform chromitites along the direction parallel to the long axis of the chromites would be higher than those along the direction parallel to the minor axis because the interconnectivity of chromites along the long axis might be better than that along the minor axis. Therefore, we proposed that the directional alignment of podiform chromitites might be a possible influencing factor on the electrical anisotropy in the upper mantle.

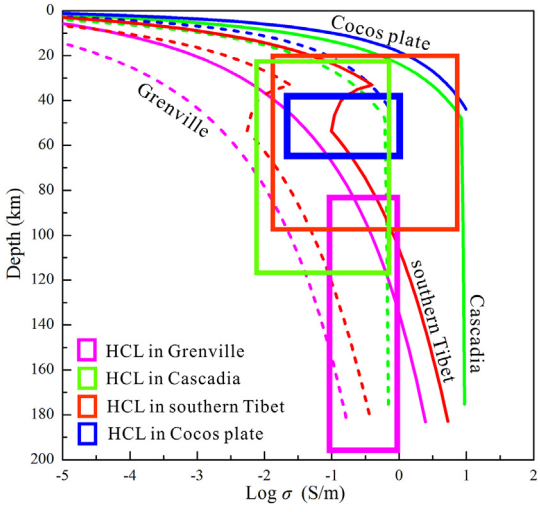

Fig. 12. Laboratory-based conductivity-depth profiles constructed from data obtained for the DS34 and DS37 runs in this study based on the thermal structure in southern Tibet, the Cocos plate, Grenville Front, and Cascadia (Mareschal et al., 1998; Currie et al., 2002, 2004; Wang et al., 2013a,b) and comparisons with MT data from these geological environments (Naif et al., 2013; Evans et al., 2014; Adetunji et al., 2015; Wang et al., 2017). The dashed/solid green, blue, purple, and red lines represent the conductivity–depth profiles for DS34/DS37 in Cascadia, the Cocos plate, Grenville Front, and southern Tibet, respectively. The green, blue, purple, and red rectangle regions display the electrical structures of Cascadia, the Cocos plate, Grenville Front, and southern Tibet, respectively.

6. Conclusions

The electrical conductivities of polycrystalline olivine–chromite systems significantly increased with increasing temperature (873–1223 K) and slightly increased with increasing pressure (1.0–3.0 GPa). The chromite content has an important effect on the conductivities of the olivine aggregates. Interconnected chromites (≥16 vol.%) dramatically enhanced the conductivities of polycrystalline olivine–chromite systems,

with increases of more than 2 orders of magnitude compared with the conductivities of pure olivine aggregates (10^{-5}–10^{-3} S/m). The activation enthalpies for the polycrystalline olivine–chromite systems with interconnected chromite (0.48–0.54 eV) were much lower than those for pure olivine (1.25 eV) and moderately lower than those of the olivine–chromite systems with isolated chromite (0.78–0.87 eV). Small polaron conduction was proposed as the conduction mechanism for the pure olivine aggregates, pure chromite aggregates, and polycrystalline olivine–chromite systems. The presence of chromites with good interconnectivity might be related to the high conductivity anomalies and electrical anisotropy in the subduction zones. In reality, it might be impossible that interconnected chromites are distributed within the tens and hundreds of kilometers depth and breadth range. Generally, there are abundant high-conductivity bodies with various volumes in a certain region. Interconnected chromites might be the dominant influencing factor of some high-connectivity bodies with small volume; however, aqueous fluids and melts possibly play the most important role for high-connectivity bodies with large volume.

Declaration of competing interest

The authors declare that they have no known competing financial interests or personal relationships that could have appeared to influence the work reported in this paper.

Acknowledgements

This research was financially supported by NSF of China (Grant Nos. 42072055, 41774099 and 41772042), Youth Innovation Promotion Association of CAS (Grant No. 2019390), Special Fund of the West Light Foundation of CAS and well as Special Fund from Shandong Provincial Key Laboratory of Water and Soil Conservation and Environmental Protection.

References

Adetunji, A.Q., Ferguson, I.J., Jones, A.G., 2015. Reexamination of magnetotelluric responses and electrical anisotropy of the lithospheric mantle in the Grenville Province, Canada. J. Geophys. Res. Solid Earth 120, 1890–1908. https://doi.org/10.1002/2014JB011713.

Arai, S., 2010. Possible recycled origin for ultrahigh-pressure chromitites in ophiolites. J. Mineral. Petrol. Sci. 105, 280–285. https://doi.org/10.2465/jmps.100622a.

Arai, S., 2013. Conversion of low-pressure chromitites to ultrahigh-pressure chromitites by deep recycling: a good inference. Earth Planet. Sci. Lett. 379, 81–87. https://doi.org/10.1016/j.epsl.2013.08.006.

Arai, S., Miura, M., 2016. Formation and modification of chromitites in the mantle. Lithos 264, 277–295. https://doi.org/10.1016/j.lithos.2016.08.039.

Arguin, J.P., Pagé, P., Barnes, S.J., Yu, S.Y., Song, X.Y., 2016. The effect of chromite crystallization on the distribution of osmium, iridium, ruthenium and rhodium in picritic magmas: an example from the Emeishan Large Igneous Province, Southwestern China. J. Petrol. 57, 1019–1048. https://doi.org/10.1093/petrology/egw033.

Baba, K., Chave, A.D., Evans, R.L., Hirth, G., Mackie, R.L., 2006. Mantle dynamics beneath the East Pacific Rise at 17°S: insights from the mantle electromagnetic and tomography (MELT) experiment. J. Geophys. Res. Solid Earth 111, B02101. https://doi.org/10.1029/2004JB003598.

Bagdassarov, N., Golabek, G.J., Solferion, G., Schmidt, M.W., 2009. Constraints on the Fe-S melt connectivity in mantle silicates from electrical impedance measurements. Phys. Earth Planet. Inter. 177, 139–146. https://doi.org/10.1016/j.pepi.2009.08.003.

Currie, C.A., Hyndman, R.D., Wang, K., Kostoglodov, V., 2002. Thermal models of the Mexico subduction zone: implications for the megathrust seismogenic zone. J. Geophys. Res. Solid Earth 107, 2370. https://doi.org/10.1029/2001JB000886.

Currie, C.A., Wang, K., Hyndman, R.D., He, J.H., 2004. The thermal effects of steady-state slab-driven mantle flow above a subducting plate: the Cascadia subduction zone and backarc. Earth Planet. Sci. Lett. 223, 35–48. https://doi.org/10.1016/j.epsl.2004.04.020.

Dai, L.D., Karato, S.I., 2014a. High and highly anisotropic electrical conductivity of the asthenosphere due to hydrogen diffusion in olivine. Earth Planet. Sci. Lett. 408, 79–86. https://doi.org/10.1016/j.epsl.2014.10.003.

Dai, L.D., Karato, S.I., 2014b. Influence of FeO and H on the electrical conductivity of olivine. Phys. Earth Planet. Inter. 237, 73–79. https://doi.org/10.1016/j.pepi.2014.10.006.

Dai, L.D., Karato, S.I., 2014c. The effect of pressure on the electrical conductivity of olivine. Phys. Earth Planet. Inter. 232, 51–56. https://doi.org/10.1016/j.pepi.2014.03.010.

Dai, L.D., Karato, S.I., 2014d. Influence of oxygen fugacity on the electrical conductivity of hydrous olivine: implications for the mechanism of conduction. Phys. Earth Planet. Inter. 232, 57–60. https://doi.org/10.1016/j.pepi.2014.04.003.

Dai, L.D., Karato, S.I., 2020. Electrical conductivity of Ti-bearing hydrous olivine aggregates at high temperature and high pressure. J. Geophys. Res. Solid Earth 125 (1). https://doi.org/10.1029/2020JB020309 e2020JB020309.

Dai, L.D., Li, H.P., Hu, H.Y., Shan, S.M., 2008. Experimental study of grain boundary electrical conductivities of dry synthetic peridotite under high-temperature, high-pressure, and different oxygen fugacity conditions. J. Geophys. Res. Solid Earth 113, B12211. https://doi.org/10.1029/2008JB005820.

Dai, L.D., Li, H.P., Li, C.H., Hu, H.Y., Shan, S.M., 2010. The electrical conductivity of dry polycrystalline olivine compacts at high temperatures and pressures. Mineral. Mag. 74, 849–857. https://doi.org/10.1180/minmag.2010.074.5.849.

Dai, L.D., Hu, H.Y., Li, H.P., Wu, L., Hui, K.S., Jiang, J.J., Sun, W.Q., 2016. Influence of temperature, pressure, and oxygen fugacity on the electrical conductivity of dry eclogite, and geophysical implications. Geochem. Geophys. Geosyst. 17, 2394–2407. https://doi.org/10.1002/2016GC006282.

Dai, L.D., Sun, W.Q., Li, H.P., Hu, H.Y., Wu, L., Jiang, J.J., 2018. Effect of chemical composition on the electrical conductivity of gneiss at high temperatures and pressures. Solid Earth 9, 233–245. https://doi.org/10.5194/se-9-233-2018.

Dai, L.D., Hu, H.Y., Sun, W.Q., Li, H.P., Liu, C.C., Wang, M.Q., 2019. Influence of high conductive magnetite impurity on the electrical conductivity of dry olivine aggregates at high temperature and high pressure. Minerals 9, 44. https://doi.org/10.3390/min9010044.

Dai, L.D., Hu, H.Y., Jiang, J.J., Sun, W.Q., Li, H.P., Wang, M.Q., Vallianatos, F., Saltas, V., 2020. An overview of the experimental studies on the electrical conductivity of major minerals in the upper mantle and transition zone. Materials 13, 408. https://doi.org/10.3390/ma13020408.

Dickey, J.S., 1975. Hypothesis of origin for podiform chromite deposits. Geochim. Cosmochim. Acta 39, 6–7. https://doi.org/10.1016/0016-7037(75)90047-2.

Evans, R.L., Wannamaker, P.E., McGary, R.S., Elsenbeck, J., 2014. Electrical structure of the central Cascadia subduction zone: the EMSLAB Lincoln Line revisited. Earth Planet. Sci. Lett. 402, 265–274. https://doi.org/10.1016/j.epsl.2013.04.021.

Gaillard, F., Malki, M., Iacono-Marziano, G., Pichavant, M., Scaillet, B., 2008. Carbonatite melts and electrical conductivity in the asthenosphere. Science 322, 1363–1365. https://doi.org/10.1126/science.1164446.

Griffin, W.L., Afonso, J.C., Belousova, E.A., Gain, S.E., Gong, X.H., González-Jiménez, J.M., Howell, D., Huang, J.X., McGowan, N., Pearson, N.J., Satsukawa, T., Shi, R., Williams, P., Xiong, Q., Yang, J.S., Zhang, M., O'Reilly, S.Y., 2016. Mantle recycling: transition zone metamorphism of Tibetan ophiolitic peridotites and its tectonic implications. J. Petrol. 57, 655–684. https://doi.org/10.1093/petrology/egw011.

Guo, H.H., Keppler, H., 2019. Electrical conductivity of NaCl-bearing aqueous fluids to 900 °C and 5 GPa. J. Geophys. Res. Solid Earth 124, 1397–1411. https://doi.org/10.1029/2018JB016658.

Guo, X., Zhang, L., Su, X., Mao, Z., Gao, X.Y., Yang, X.Z., Ni, H.W., 2018. Melting inside the Tibetan Crust? Constraint from electrical conductivity of peraluminous granitic melt. Geophys. Res. Lett. 45, 3906–3913. https://doi.org/10.1029/2018GL077804.

Hashin, Z., Shtrikman, S., 1962. A variational approach to the theory of the effective magnetic permeability of multiphase materials. J. Appl. Phys. 33, 3125–3131. https://doi.org/10.1063/1.1728579.

Hirsch, L.M., Shankland, T.J., Duba, A.G., 1993. Electrical conduction and polaron mobility in Fe-bearing olivine. Geophys. J. Int. 114, 36–44. https://doi.org/10.1111/j.1365-246X.1993.tb01464.x.

Hu, H.Y., Dai, L.D., Li, H.P., Jiang, J.J., Hui, K.S., 2014. Electrical conductivity of K-feldspar at high temperature and high pressure. Mineral. Petrol. 108, 609–618. https://doi.org/10.1007/s00710-014-0325-7.

Hu, H.Y., Dai, L.D., Li, H.P., Jiang, J.J., Hui, K.S., Li, J., 2015. Temperature and pressure dependence of electrical conductivity in synthetic anorthite. Solid State Ionics 276. https://doi.org/10.1016/j.ssi.2015.04.008 136–14.

Hu, H.Y., Dai, L.D., Li, H.P., Hui, K.S., Sun, W.Q., 2017. Influence of dehydration on the electrical conductivity of epidote and implications for high conductivity anomalies in subduction zones. J. Geophys. Res. Solid Earth 122, 2751–2762. https://doi.org/10.1002/2016JB013767.

Hu, H.Y., Dai, L.D., Li, H.P., Sun, W.Q., Li, B.S., 2018. Effect of dehydrogenation on the electrical conductivity of Fe-bearing amphibole: implications for high conductivity anomalies in subduction zones and continental crust. Earth Planet. Sci. Lett. 498, 27–37. https://doi.org/10.1016/j.epsl.2018.06.003.

Hui, K.S., Zhang, H., Li, H.P., Dai, L.D., Hu, H.Y., Jiang, J.J., Sun, W.Q., 2015. Experimental study on the electrical conductivity of quartz andesite at high temperature and high pressure: evidence of grain boundary transport. Solid Earth 6, 1037–1043. https://doi.org/10.5194/se-6-1037-2015.

Kapsiotis, A., Rassios, A.E., Uysal, I., Grieco, G., Akmas, R.M., Saka, S., Bussolesi, M., 2018. Compositional fingerprints of chromian spinel from the refractory chrome ores of Metalleion, Orthris (Greece): implications for metallogeny and deformation of chromitites within a "hot" oceanic fault zone. J. Geochem. Explor. 185, 14–32. https://doi.org/10.1016/j.gexplo.2017.11.003.

Karato, S.I., 2013. Theory of isotope diffusion in a material with multiple species and its implications for hydrogen-enhanced electrical conductivity in olivine. Phys. Earth Planet. Inter. 219, 49–54. https://doi.org/10.1016/j.pepi.2013.03.001.

Karato, S.I., 2019. Some remarks on hydrogen-assisted electrical conductivity in olivine and other minerals. Prog. Earth Planet. Sci. 6, 55. https://doi.org/10.1186/s40645-019-0301-2.

Kim, Y.S., Yin, J.W., Kim, P., Jong, C., Kim, U., Kim, C., 2020. The Ryonchon podiform chromitite from the Chongjin ophiolite. Ore Geol. Rev. 127, 103718. https://doi.org/10.1016/j.oregeorev.2020.103718.

Laumonier, M., Gaillard, F., Sifre, D., 2015. The effect of pressure and water concentration on the electrical conductivity of dacitic melts: implication for the magnetotelluric imaging in subduction areas. Chem. Geol. 418, 66–76. https://doi.org/10.1016/j.chemgeo.2014.09.019.

Laumonier, M., Farla, R., Frost, D.J., Katsura, T., Marquardt, K., Bouvier, A.S., Baumgartner, L.P., 2017. Experimental determination of melt interconnectivity and electrical conductivity in the upper mantle. Earth Planet. Sci. Lett. 463, 286–297. https://doi.org/10.1016/j.epsl.2017.01.037.

Li, X., Ma, X.B., Chen, Y., Xue, S., Varentsov, I.M., Bai, D.H., 2020. A plume-modified lithospheric barrier to the southeastward flow of partially molten Tibetan crust inferred from magnetotelluric data. Earth Planet. Sci. Lett. 548, 116493. https://doi.org/10.1016/j.epsl.2020.116493.

Lin, J.F., Speziale, S., Mao, Z., Marquardt, H., 2013. Effects of the electronic spin transitions of iron in lower mantle minerals: implications for deep mantle geophysics and geochemistry. Rev. Geophys. 51, 244–275. https://doi.org/10.1002/rog.20010.

Liu, X., Dai, L.D., Deng, L.W., Fan, D.W., Liu, Q., Ni, H.W., Sun, Q., Wu, X., Yang, X.Z., Zhai, S.M., Zhang, B.H., Zhang, L., Li, H.P., 2017. Recent progresses in some fields of high-pressure physics relevant to Earth sciences achieved by Chinese scientists. Chin. J. High Press. Phys. 31, 657–681. https://doi.org/10.11858/gywlxb.2017.06.001 (in Chinese with English abstract).

Manthilake, G., Mookherjee, M., Bolfan-Casanova, N., Andrault, D., 2015. Electrical conductivity of lawsonite and dehydrating fluids at high pressures and temperatures. Geophys. Res. Lett. 42, 7398–7405. https://doi.org/10.1002/2015GL064804.

Liu, X., O'Neill, H.St.C., 2004. The effect of Cr_2O_3 on the partial melting of spinel lherzolite in the system CaO–MgO–Al_2O_3–SiO_2–Cr_2O_3 at 1.1 GPa. J. Petrol. 45, 2261–2286. https://doi.org/10.1093/petrology/egh055.

Manthilake, G., Bolfan-Casanova, N., Novella, D., Mookherjee, M., Andrault, D., 2016. Dehydration of chlorite explains anomalously high electrical conductivity in the mantle wedges. Sci. Adv. 2, e1501631. https://doi.org/10.1126/sciadv.1501631.

Mareschal, J.C., Jaupart, C., Cariépy, C., Cheng, L.Z., Guillou-Frottier, L., Bienfait, G., Lapointe, R., 1998. Heat flow and deep thermal structure near the southeastern edge of the Canadian Shield. Can. J. Earth Sci. 37, 399–414. https://doi.org/10.1139/e98-106.

Matsuno, T., Seama, N., Evan, R.L., Chave, A.D., Baba, K., White, A., Goto, T., Heinson, G., Boren, G., Yoneda, A., Utada, H., 2010. Upper mantle electrical resistivity structure beneath the central Mariana subduction system. Geochem. Geophys. Geosyst. 11, Q09003. https://doi.org/10.1029/2010GC003101.

Matsuno, T., Bada, K., Utada, H., 2020. Probing 1-D electrical anisotropy in the oceanic upper mantle from seafloor magnetotelluric array data. Geophys. J. Int. 222, 1502–1525. https://doi.org/10.1093/gji/ggaa221.

Matveev, S., Ballhaus, C., 2002. Role of water in the origin of podiform chromitite deposits. Earth Planet. Sci. Lett. 203, 235–243. https://doi.org/10.1016/S0012-821X(02)00860-9.

McGowan, N.M., Griffin, W.L., González-Jiménez, J.M., Belousova, E., Afonso, J.C., Shi, R., McCammon, C.A., Pearson, N.J., O'Reilly, S.Y., 2015. Tibetan chromitites: excavating the slab graveyard. Geology 43, 179–182. https://doi.org/10.1130/G36245.1.

Naif, S., Key, K., Constable, S., Evans, R.L., 2013. Melt-rich channel observed at the lithosphere–asthenosphere boundary. Nature 495, 356–359. https://doi.org/10.1038/nature11939.

Padilha, A.L., Vitorello, I., Antunes, C.E., Padua, M.B., 2015. Imaging three-dimensional crustal conductivity structures reflecting continental flood basalt effects hidden beneath thick intracratonic sedimentary basin. J. Geophys. Res. Solid Earth 120, 4702–4719. https://doi.org/10.1002/2014JB011657.

Page, P., Barnes, S.J., 2009. Using trace elements in chromites to constrain the origin of podiform chromitites in the Thetford mines ophiolite, Quebec, Canada. Econ. Geol. 104, 997–1018. https://doi.org/10.2113/econgeo.104.7.997.

Pommier, A., Leinenweber, K., Kohlstedt, D.L., Qi, C., Garbero, E.J., Mackwell, S.J., Tyburczy, J.A., 2015. Experimental constraints on the electrical anisotropy of the lithosphere-asthenosphere system. Nature 522, 202–208. https://doi.org/10.1038/nature14502.

Pommier, A., Kohlstedt, D.L., Hansen, L.N., Mackwell, S., Tasaka, M., Heidelbach, F., Leinenweber, K., 2018. Transport properties of olivine grain boundaries from electrical experiments. Contrib. Mineral. Petrol. 173, 41. https://doi.org/10.1007/s00410-018-1468-z.

Ringwood, A.E., 1975. Composition and Petrology of the Earth's Mantle. McGraw Hill, New York, pp. 231–249.

Ringwood, A.E., 1982. Phase transformations and differentiation in subducted lithosphere: implications for mantle dynamics, basalt petrogenesis and crustal evolution. J. Geol. 90, 611–643. https://doi.org/10.1086/628721.

Roberts, J.J., Tyburczy, J.A., 1991. Frequency dependent electrical properties of polycrystalline olivine compacts. J. Geophys. Res. Solid Earth 96, 16205–16222. https://doi.org/10.1029/91JB01574.

Rollinson, H., Mameri, L., Barry, T., 2018. Polymineralic inclusions in mantle chromitites from the Oman ophiolite indicate a highly magnesian parental melt. Lithos 310, 381–391. https://doi.org/10.1016/j.lithos.2018.04.024.

Satsukawa, T., Griffin, W.L., Piazolo, S., O'Reilly, S.Y., 2015. Messengers from the deep: fossil wadsleyite–chromite microstructures from the mantle transition zone. Sci. Rep. 5, 16484. https://doi.org/10.1038/srep16484.

Schock, R.N., Duba, A.G., Shankland, T.J., 1989. Electrical conduction in olivine. J. Geophys. Res. Solid Earth 94, 5829–5839. https://doi.org/10.1029/JB094iB05p05829.

Shen, K.W., Wang, D.J., Liu, T., 2020. Electrical conductivity of amphibolite at high temperature and high pressure and its geophysical implications. Chinese. J. Geophys. 63, 3398–3408. https://doi.org/10.6038/cjg2020N0461.

Sun, W.Q., Dai, L.D., Li, H.P., Hu, H.Y., Wu, L., Jiang, J.J., 2017. Electrical conductivity of mudstone (before and after dehydration at high P–T) and a test of high conductivity layers in the crust. Am. Mineral. 102, 2450–2456. https://doi.org/10.2138/am-2017-6146.

Sun, W.Q., Dai, L.D., Li, H.P., Hu, H.Y., Jiang, J.J., Wang, M.Q., 2020. Electrical conductivity of clinopyroxene–NaCl–H_2O system at high temperatures and pressures: implications for high conductivity anomalies in the deep crust and subduction zone. J. Geophys. Res. Solid Earth 125. https://doi.org/10.1029/2019JB019093 e2019JB019093.

ten Grotenhuis, S.M., Drury, M.R., Peach, C.J., Spiers, C.J., 2004. Electrical properties of fine-grained olivine: evidence for grain boundary transport. J. Geophys. Res. Solid Earth 109, B06203. https://doi.org/10.1029/2003JB002799.

Thayer, T.P., 1964. Principal features and origin of podiform chromite deposits, and some observations on the Guleman–Soridag district, Turkey. Econ. Geol. 59, 1497–1524. https://doi.org/10.2113/gsecongeo.59.8.1497.

Torabi, G., 2009. Chromitite potential in mantle peridotites of the Jandaq ophiolite (central Iran) Les Péridotites de l'ophiolite de Jandaq (Iran central) peuvent-elles renfermer des gisements de chromite? Compt. Rendus Geosci. 341, 982–992. https://doi.org/10.1016/j.crte.2009.07.014.

Uysal, I., Kapsiotis, A., Akmaz, R.M., Saka, S., Seitz, H.M., 2018. The Guleman ophiolitic chromitites (SE Turkey) and their link to a compositionally evolving mantle source during subduction initiation. Ore Geol. Rev. 93, 98–113. https://doi.org/10.1016/j.oregeorev.2017.12.017.

Wang, D.J., Li, H.P., Matsuzaki, T., Yoshino, T., 2010. Anisotropy of synthetic quartz electrical conductivity at high pressure and temperature. J. Geophys. Res. Solid Earth 115, B09211. https://doi.org/10.1029/2009JB006695.

Wang, C.Y., Chen, W.P., Wang, L.P., 2013a. Temperature beneath Tibet. Earth Planet. Sci. Lett. 375, 326–337. https://doi.org/10.1016/j.epsl.2013.05.052.

Wang, D.J., Karato, S.I., Jiang, Z.T., 2013b. An experimental study of the influence of graphite on the electrical conductivity of olivine aggregates. Geophys. Res. Lett. 40, 2028–2032. https://doi.org/10.1002/grl.50471.

Wang, G., Wei, W.B., Ye, G.F., Jing, J.N., Zhang, L.T., Dong, H., Xie, C.L., Omisore, B.O., Guo, Z.Q., 2017. 3-D electrical structure across the Yadong-Gulu rift revealed by magnetotelluric data: new insights on the extension of the upper crust and the geometry of the underthrusting Indian lithospheric slab in southern Tibet. Earth Planet. Sci. Lett. 474, 172–179. https://doi.org/10.1016/j.epsl.2017.06.027.

Wei, W., Unsworth, M., Jones, A.G., Booker, J., Tan, H., Nelson, D., Chen, L., Li, S., Solon, K., Bedrosian, P., Jin, S., Deng, M., Ledo, J., Kay, D., Roberts, B., 2001. Detection of widespread fluids in the Tibetan crust by magnetotelluric studies. Science 292, 716–718. https://doi.org/10.1126/science.1010580.

Xiao, Q.B., Zhang, J., Zhao, G.Z., Wang, J.J., 2013. Electrical resistivity structures northeast of the eastern Kunlun fault in the northeastern Tibet: tectonic implications. Tectonophysics 601, 125–138. https://doi.org/10.1016/j.tecto.2013.05.003.

Xie, C.L., Jin, S., Wei, W.B., Ye, G.F., Jing, J.E., Zhang, L.T., 2016. Crustal electrical structures and deep processes of the eastern Lhasa terrane in the south Tibetan plateau as revealed by magnetotelluric data. Tectonophysics 675, 168–180. https://doi.org/10.1016/j.tecto.2016.03.017.

Xu, Y.S., McCammon, C., 2002. Evidence for ionic conductivity in lower mantle (Mg,Fe)(Si, Al)O_3 perovskite. J. Geophys. Res. Solid Earth 107, B102251. https://doi.org/10.1029/2001JB000677.

Xu, Y.S., Shankland, T.J., Duba, A.G., 2000. Pressure effect on electrical conductivity of mantle olivine. Phys. Earth Planet. Inter. 118, 149–161. https://doi.org/10.1016/S0031-9201(99)00135-1.

Yamamoto, S., Komiya, T., Hirose, K., Maruyama, S., 2009. Coesite and clinopyroxene exsolution lamellae in chromites: in-situ ultrahigh-pressure evidence from podiform chromitites in the Luobusa ophiolite, southern Tibet. Lithos 109, 314–322. https://doi.org/10.1016/j.lithos.2008.05.003.

Yang, J.S., Bai, W.J., Fang, Q.S., Meng, F.C., Chen, S.Y., Zhang, Z.M., Rong, H., 2007. Discovery of diamond and an unusual mineral group from the podiform chromite, Polar Ural. Geol. China 34, 950–952 (in Chinese with English abstract).

Zhang, Z., Pommier, A., 2017. Electrical investigation of metal–olivine systems and application to the deep interior of mercury. J. Geophys. Res. Planets 122, 2702–2718. https://doi.org/10.1002/2017JE005390.

Zhang, R.Y., Yang, J.S., Ernst, W.G., Jahn, B.M., Lizuka, Y., Guo, G.L., 2016. Discovery of in situ super-reducing, ultrahigh-pressure phases in the Luobusa ophiolitic chromitites, Tibet: new insights into the deep upper mantle and mantle transition zone. Am. Mineral. 101, 1285–1294. https://doi.org/10.2138/am-2016-5436.

Zhang, Y.F., Jin, Z.M., Griffin, W.L., Wang, C., Wu, Y., 2017. High-pressure experiments provide insights into the Mantle Transition Zone history of chromitite in Tibetan ophiolites. Earth Planet. Sci. Lett. 463, 151–158. https://doi.org/10.1016/j.epsl.2017.01.036.

Zhang, P.F., Zhou, M.F., Malpas, J., Robinson, P.T., 2020. Origin of high-Cr chromite deposits in nascent mantle wedges: petrological and geochemical constraints from the Neo-Tethyan Luobusa ophiolite, Tibet. Ore Geol. Rev. 123, 103581. https://doi.org/10.1016/j.oregeorev.2020.103581.

Zhou, M.F., Robinson, P.T., Malpas, J., Li, Z.J., 1996. Podiform chromitites in the Luobusa ophiolite (southern Tibet): implications for melt–rock interaction and chromite segregation in the upper mantle. J. Petrol. 37, 3–21. https://doi.org/10.1093/petrology/37.1.3.

Zhou, M.F., Robinson, R.T., Su, B.X., Gao, J.F., Li, J.W., Yang, J.S., Malpas, J., 2014. Compositions of chromite, associated minerals, and parental magmas of podiform chromite deposits: the role of slab contamination of asthenospheric melts in suprasubduction zone environments. Gondwana Res. 26, 262–283. https://doi.org/10.1016/j.gr.2013.12.011.